

# Strong Backscatterer at the Edge of a Two-dimensional Topological Insulator

Jun-Hui Zheng<sup>1,2</sup> and Miguel A. Cazalilla<sup>2,3,4</sup>

<sup>1</sup>*Institut für Theoretische Physik, Goethe-Universität, 60438 Frankfurt/Main, Germany.*

<sup>2</sup>*Department of Physics, National Tsing Hua University, Hsinchu 30013, Taiwan.*

<sup>3</sup>*National Center for Theoretical Sciences (NCTS), Hsinchu 30013, Taiwan.*

<sup>4</sup>*Donostia International Physics Center (DIPC),*

*Manuel de Lardizabal, 4. 20018, San Sebastian, Spain.*

We study the problem of a backscattering impurity coupled to the edge states of a two-dimensional topological insulator. In the regime where the backscattering potential is larger than the band gap and accounting for electron-electron interactions, it is shown that the system can be described as a resonant level coupled to the one-dimensional (1D) channel of interacting edge electrons. We discuss the relationship of this system to the model of a (structureless) impurity in a 1D interacting electron liquid. Different from the latter model, in the resonant regime transmission is suppressed also for weak to moderately attractive interactions.

PACS numbers: 21.XX

At zero temperature, charge transport in two-dimensional topological insulators (2DTI) takes place through 1D edge states, whose metallic character is protected by symmetry [1–4]. For instance, time reversal symmetry (TRS) prevents the ubiquitous Anderson localization from happening in the 1D edge channels of quantum spin Hall insulators (QSHI) in the presence of scalar and spin-orbit (SO) disorder, and for weak to moderate interactions [2–5].

The QSH effect exhibited by QSHI has been observed in HgTe/CdTe and InAs/GaSb/AlSb quantum wells [6]. However, for longer ( $\sim 1 \mu\text{m}$ ) edge channels, deviations from the expected conductance quantization of  $2e^2/h$  and relatively short mean-free paths have been measured [6]. Despite intense theoretical investigation [4, 7] on the backscattering (BS) mechanisms, a complete understanding of the origin of the finite edge channel resistance has not been achieved. The proposed mechanisms involve electron-electron scattering, often in combination with scalar, SO, or magnetic disorder [5, 7–9]. Magnetic impurities break TRS (above the Kondo temperature) and lead to BS [2, 8, 10, 11]. Yet, whether electron BS yields or not corrections to the DC conductance depends on the microscopic details of the scatterer [4, 8–10].

For the simplest model of an impurity inducing BS in

an interacting 1D channel, Kane and Fisher found [12–14] that repulsive electron interactions enhance BS whereas attractive interactions suppress it. In the latter case, the impurity potential is screened and the channel becomes perfectly transparent as the temperature  $T \rightarrow 0$ . For repulsive interactions, the channel is effectively cut in two as  $T \rightarrow 0$  by the renormalization to strong coupling of the BS potential. Many of Kane and Fisher’s predictions have been confirmed numerically [15], analytically using the Bethe ansatz [16], and experimentally using carbon nanotubes [17]. For weak interactions, Yue, Mateev and Glazman [13, 14, 18] obtained a complementary description by relying on the Hartree-Fock approximation: the Friedel oscillations introduced by the impurity in the electron density modify the scattering potential, leading to a logarithmic singularity  $\sim \log |k - k_F|$  in the reflection coefficient. The logarithm is just the first term in an infinite series which, upon resummation, yields the powerlaw conductance obtained by Kane and Fisher [13, 18].

In this article, we will address the question of under which conditions the 1D description studied by Kane and Fisher description applies to a backscatterer coupled to the edge states of a 2DTI (see Fig. 1). Specifically, we show the latter scenario does not universally apply and provide an alternative low-energy model. As shown below, the physics of an BS impurity in a 2DTI is different due to the new features brought about by the dimensionality and electronic structure of the TI. Unlike earlier work [19], our focus is on the effective model describing the low-energy physics in the presence of interactions, which have dramatic effects in 1D systems [20].

Indeed, for a strong impurity potential in the bulk of a TI, bound states appear within the band gap [21]. This also happens for large spin  $S$  magnetic impurity (or a magnetic cluster), at temperatures  $T$  well above the Kondo temperature  $T_K$  ( $T_K$  is suppressed for large  $S$  [22]). The impurity will be treated as a local Zeeman field, whose direction, in order to maximize BS, we shall

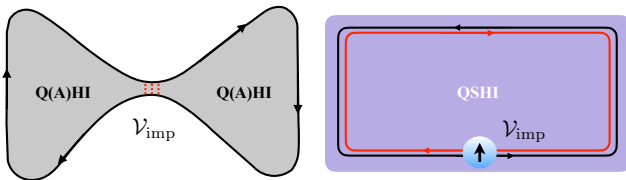


FIG. 1. (Color online) Sketch of two possible realizations of the system studied here: (Right) a large-spin magnetic impurity (or magnetic cluster) in a quantum spin-Hall insulator (QSHI) (Left) a *strongly coupled* quantum point contact in a quantum (anomalous) Hall insulator (Q(A)HI).

take perpendicular to the spin quantization axis:

$$\mathcal{V}_{\text{imp}} = \lambda_{\text{imp}} (c_{i_0\uparrow}^\dagger c_{i_0\downarrow} + \text{h.c.}) = \lambda_{\text{imp}} c_{i_0}^\dagger s^x c_{i_0}. \quad (1)$$

where  $c_i^\dagger = (c_{i\uparrow}^\dagger, c_{i\downarrow}^\dagger)$  creates one electron at lattice site  $\mathbf{R}_i$ . Here, we are interested in the limit where  $\lambda_{\text{imp}}$  is larger than the band gap. The resulting problem is by no means of academic interest as the size of the band gap of 2DTI can be made rather small [4, 6], especially close to the topological transition. For an BS impurity in a QSHI sufficiently far from the edge, the potential (1) leads to two (bound) states within the gap. As the impurity moves from the bulk to the edge, the bound states resonate with the edge states. Thus, the BS impurity problem at the edge of a 2DTI a problem is akin to a resonant level problem coupled to a 1D interacting channel [12, 18, 23–26].

Before describing the derivation of the above picture, it is worth mentioning that, besides a strongly interacting magnetic impurity at the edge of a QSH insulator, the model considered here also describes a strongly-coupled point contact in a quantum (anomalous) Hall insulator (cf. Fig. 1). This system may be also realized in a point contact in a photonic topological material, e.g. Ref. 27.

In order to describe the QSHI, we shall use the Kane-Mele (KM) model [28], which is defined on a honeycomb lattice by the Hamiltonian:

$$H_0 = -t \sum_{\langle i,j \rangle} c_i^\dagger c_j - i\lambda_{\text{SO}} \sum_{\langle\langle i,j \rangle\rangle} \nu_{ij} c_i^\dagger s^z c_j \quad (2)$$

where  $\lambda_{\text{SO}}$  describes the *intrinsic* SO coupling [28] as an imaginary next nearest neighbor hopping and  $\nu_{ij} = \pm 1$  depends on the electron hopping path;  $s^z$  is the electron spin projection on the axis perpendicular to the 2D plane.

In the absence of interactions (to be treated further below), the impurity problem is described by the Hamiltonian  $H = H_0 + \mathcal{V}_{\text{imp}}$  (cf. Eqs. 1 and 2). In order to solve it, we first obtain an analytical solution of the KM model, Eq. (2) in a strip geometry of width  $L$  with the zigzag edges (Fig. 2). In this geometry, the Bloch wavevector parallel to the edge,  $k_x$ , is a good quantum number. However,  $k_y = -i\partial_y$  must be treated as an operator (see below). The wave functions along the  $y$ -axis obey open boundary conditions [29]. We first consider the Fourier transform of Eq. (2) in the Bloch basis, where:

$$c_{i \in A} = \sum_{\mathbf{k}} \frac{c_{\mathbf{k}A}}{\sqrt{N_t}} e^{i\mathbf{k} \cdot (\mathbf{R}_i + \mathbf{r}_g)}, \quad c_{i \in B} = \sum_{\mathbf{k}} \frac{c_{\mathbf{k}B}}{\sqrt{N_t}} e^{i\mathbf{k} \cdot \mathbf{R}_i}. \quad (3)$$

Here  $\mathbf{R}_{i \in A(B)}$  is the position of  $A(B)$  sublattice sites and  $N_t$  is total number of unit cells. Because of the bi-partite structure of the honeycomb lattice, the Fourier transform of  $H_0$  is not unique and depends on the relative phase  $\mathbf{k} \cdot \mathbf{r}_g$ . This gauge freedom must be fixed by the boundary conditions (BCs). The appropriate choice for the zigzag edge is  $\mathbf{r}_g = -(a/2\sqrt{3})\mathbf{e}_y$ , so that the  $N$ th row

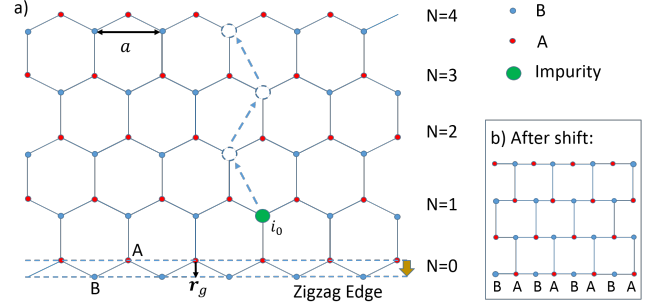


FIG. 2. (Color online) Sketch of (a) the zigzag edge with a single impurity at the edge and (b) the “brick wall” lattice to which it maps.

of the A sublattice overlaps with the  $N$ th row of the B sublattice (See Fig. 2). This maps the honeycomb lattice onto the so-called “brick wall” lattice and thus the BCs are  $\Phi = (\Phi_B, \Phi_A)^T = 0$  at  $y = \pm L/2$ . After identifying the boundary conditions, we proceed to solve the 1D Schrödinger equation:

$$\mathcal{H}_0^s(\alpha, \hat{\beta}) \Phi_s(k_x, y) = \epsilon \Phi_s(k_x, y), \quad (4)$$

where we have used the following notation:  $\hat{\beta} = -i\frac{\sqrt{3}a}{2}\partial_y$  and  $\mathcal{H}_0^s = \sum_i d_s^i \sigma^i$ , with  $d_s^x = -t(2\cos\alpha + \cos\hat{\beta})$ ,  $d_s^y = -t\sin\hat{\beta}$  and  $d_s^z = s\lambda_{\text{SO}}(2\sin 2\alpha - 4\sin\alpha\cos\hat{\beta})$ , respectively ( $\alpha = k_x a/2$ ). In addition, since  $s^z$  is a good quantum number,  $s = \pm 1$ . Below, we look for solutions that are combinations of plane waves  $e^{ik_y y}$ .

We are not interested in finite size effects and therefore we focus on the large  $L$  limit. Thus, the coupling between the two edges vanishes and we obtain the dispersion for the edge states [30]:

$$\epsilon_s(k_x) = \pm \frac{6s\lambda_{\text{SO}}t\sin(k_x a)}{\sqrt{t^2 + [4\lambda_{\text{SO}}\sin(k_x a/2)]^2}}, \quad (5)$$

where the  $+$  ( $-$ ) sign corresponds to the bottom (top) edge at  $y = -L/2$  ( $y = +L/2$ ) and  $s = \pm 1$ . The bands of edge states cross at  $k_x = \frac{\pi}{a}$  [28] (for a bearded edge they cross at  $k_x = 0$  [30, 31]). For  $k_x \approx \frac{\pi}{a}$ , Eq. (5) agrees with the results of Ref. 32. For the bottom edge states, below we use the notation  $|k_x, s\rangle$ . A plot of the bands [28] for a wide zigzag ribbon obtained by this method can be found in the supplementary material [30].

Next, we consider the form of the eigenstates. Up to a phase factor depending on  $k_x$ , they are a combination of four  $e^{ik_y y}$ , where  $k_y = \pm k_1, \pm k_2$ . There are three kinds of states: i)  $\text{Im } k_1 \neq 0$  and  $\text{Im } k_2 \neq 0$ , which is an eigenstate localized at the edge, ii)  $\text{Im } k_1 \neq 0$  and  $\text{Im } k_2 = 0$ , a resonance state, which is extended in the bulk, and iii)  $\text{Im } k_1 = 0$  and  $\text{Im } k_2 = 0$  a bulk scattering state [30].

In order to investigate the effect of the impurity on the electronic transport, we next solve the Lippmann-Schwinger equation (LSE)  $|\Psi\rangle = |\Phi\rangle + G_0(\epsilon) \mathcal{V}_{\text{imp}} |\Psi\rangle$ ,

where  $G_0(\epsilon) = (\epsilon + i0^+ - H_0)^{-1}$  is the Green's function for Eq. (2). We assume the BS impurity to be located on the B sublattice at the bottom edge since the wavefunction of edge states on this edge is mostly localized on the B sublattice [30]. In order to extract the transmission and reflection coefficient of the edge electrons, we assume the incident electron has a Bloch wave number  $k_x^0$  on the right-moving edge channel, i.e.,  $|\Phi\rangle = |k_x^0, s = -1\rangle$  and therefore its energy is  $\epsilon_-(k_x^0)$  and group velocity is  $v = \partial_{k_x} \epsilon_-(k_x)|_{k_x=k_x^0}$ . Let us introduce  $\Phi(s\sigma, \mathbf{r}) = \langle s, \sigma, \mathbf{r} | \Phi \rangle$  and  $\Psi(s\sigma, \mathbf{r}) = \langle s, \sigma, \mathbf{r} | \Psi \rangle$ , where  $\sigma = (+, -)$  corresponds to  $(B, A)$ . Thus, the asymptotic behavior of the wavefunction for  $x \rightarrow +\infty$  becomes  $|\Psi\rangle \rightarrow (1 + \zeta_t)|\Phi\rangle$  and  $|\Psi\rangle \rightarrow |\Phi\rangle + \zeta_r|\tilde{\Phi}\rangle$ , for  $x \rightarrow -\infty$ , where  $|\tilde{\Phi}\rangle = |\frac{2\pi}{a} - k_x^0, s = +1\rangle$ , and

$$\zeta_t = -i\lambda_{\text{imp}} L_x \frac{\Psi(++ , \mathbf{r}_0) \Phi^*(-+, \mathbf{r}_0)}{v}, \quad (6)$$

$$\zeta_r = -i\lambda_{\text{imp}} L_x \frac{\Psi(-+, \mathbf{r}_0) \tilde{\Phi}^*(++, \mathbf{r}_0)}{v}. \quad (7)$$

Here  $L_x$  is the normalization length of system along the edge and  $\mathbf{r}_0 \propto \mathbf{R}_{i_0}$  is the impurity position.

From the above results, the transmission and reflection coefficients can be extracted as  $\mathcal{T}(\epsilon) = |1 + \zeta_t|^2$  and  $\mathcal{R}(\epsilon) = |\zeta_r|^2$ , respectively. The energy dependence of the transmission coefficient is shown in Fig. 3. Note that, when the impurity is located on the first atomic row (i.e.  $N = 1$ ), the transmission is essentially independent on the energy, which makes it similar to a BS impurity in a purely 1D channel. This behavior arises from the weak coupling induced by the impurity between the edge and bulk states (owing to the small weight of the bulk states on the  $N = 1$  row), even for relatively large values of  $\lambda_{\text{imp}}$ . Thus, scattering is dominated by the 1D edge states. However, for the second atomic row and beyond (i.e.  $N \geq 2$ ), the weight of the bulk-state wavefunctions becomes larger, thus increasing the coupling between bulk and edge states. For large values of  $\lambda_{\text{imp}}$ , a pair of narrow scattering resonances appears within the gap. In the neighborhood of the anti-resonances the transmission coefficient changes very rapidly with energy and (on resonance) vanishes for large  $\lambda_{\text{imp}}$ .

In order to understand the emergence of a pair of scattering anti-resonances, we need to consider the poles of the T-matrix:  $T(\epsilon) = [1 - \mathcal{V}_{\text{imp}} G_0(\epsilon)]^{-1} \mathcal{V}_{\text{imp}}$ . For a strong impurity potential located within the bulk, far from the edge, the impurity only couples to the bulk states. In this case, the poles of the T-matrix are obtained from the condition  $\det[1 - \lambda_{\text{im}} G_0^B(\mathbf{r}_0, \mathbf{r}_0, \epsilon) s^x] = 0$  where  $G_0^B$  is the Green's function in the bulk. The latter is real for  $\epsilon$  within the energy gap since the density of states vanishes and it is odd in  $\epsilon$  (due to the particle-hole symmetry of  $H_0$ ), therefore vanishing at  $\epsilon = 0$ . Thus,  $G_0^B(\mathbf{r}_0, \mathbf{r}_0, \epsilon) \sim \epsilon$  for small  $\epsilon$ . Hence, at large  $\lambda_{\text{imp}}$ , two bound states, appear at  $\epsilon \simeq \pm(\lambda_{\text{imp}})^{-1}$  corresponding to the two eigenvalues of  $s^x$ . As the impurity

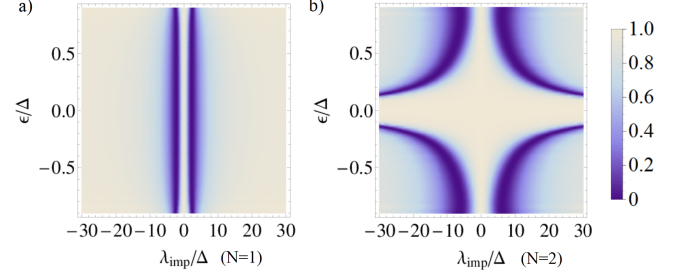


FIG. 3. Transmission coefficient  $\mathcal{T}(\epsilon)$  for an impurity on a B sublattice site on (a) the first atomic row (i.e.,  $N = 1$ ) and (b)  $N = 2$ . (The spin-orbit coupling is  $\lambda_{\text{SO}} = 0.06 t$ .)

location approaches the edge, the bound states will hybridize with the continuum of edge states, leading to the anti-resonances in the transmission coefficient.

In the following, we shall construct a 1D low-energy effective model that describes the edge channels in the presence of the BS impurity at large  $\lambda_{\text{imp}}/\Delta$ , where  $\Delta = 3\sqrt{3}\lambda_{\text{SO}}$  is bulk band gap. The effective model is valid at energies and temperatures smaller than  $\Delta$  and therefore only involves the edge degrees of freedom. The construction of the effective low energy model is aided by using the known symmetries of the system Hamiltonian,  $H = H_0 + \mathcal{V}_{\text{imp}}$ , as both share the same symmetries. To this end, we note that the KM model in the strip geometry,  $H_0$ , is invariant under TRS ( $\mathcal{T}$ ), spin rotations about the  $z$ -axis (i.e.  $U_\theta = \exp(-i\theta s^z/2)$ ,  $U_\theta^{-1} H_0 U_\theta = H_0$ ), particle-hole symmetry ( $\mathcal{C}$ ), and translations by multiples of  $a$  along the edge direction. The impurity potential,  $\mathcal{V}_{\text{imp}}$ , breaks all those symmetries, but the composite system described by  $H$  is invariant under the subgroup span by the combined  $U_\pi \mathcal{T}$  and  $\mathcal{C} \mathcal{T}$  transformations. Therefore, according to the above discussion, the effective model takes the form of a Fano model [33] describing two discrete levels coupled to the continuum of edge states, which is invariant under  $U_\pi \mathcal{T}$  and  $\mathcal{C} \mathcal{T}$ . Since for  $|\lambda_{\text{imp}}| \rightarrow \infty$  the position of the resonances approaches the center of the band gap at  $\epsilon = 0$ , we shall focus in the neighborhood of  $k_x = \frac{\pi}{a}$ , where linearization the edge state spectrum, i.e.  $\epsilon_\pm(k_x) = \mp v_F k$ , is a good approximation. Thus, the effective Hamiltonian reads

$$H_{\text{eff}} = H_B + H_+ [u, t_+ \psi(0)] + H_- [d, t_- \psi(0)], \quad (8)$$

$$H_B = i v_F \int dx \psi^\dagger s^z \partial_x \psi + V_B a_0 \psi^\dagger(0) s^x \psi(0), \quad (9)$$

$$H_\pm [f, \chi] = \pm \epsilon_0 (f^\dagger f - \frac{1}{2}) + V_c a_0^{1/2} [f^\dagger \chi + \text{h.c.}] \quad (10)$$

where  $\psi^\dagger(x) = (\psi_L^\dagger(x), \psi_R^\dagger(x))$  is the spinor field operator describing the edge states,  $u^\dagger$  and  $d^\dagger$  are the creation operators of electrons in the bound states with  $s^x$  eigenvalue and energy  $s^x = +1, \epsilon = +\epsilon_0$  and  $s^x = -1, \epsilon = -\epsilon_0$ , respectively, and  $t_\pm = (\pm 1, 1)$ ;  $a_0 = v_F/\Delta$  is a short distance cut-off. In the above model,  $V_B$  describes a renor-

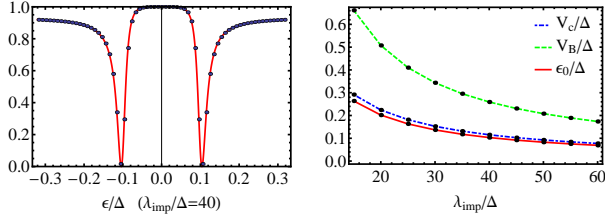


FIG. 4. (Color online) (Left) Transmission coefficient for an impurity strength  $\lambda_{\text{imp}} = 40 \Delta$  ( $\Delta$  is the band gap). Dots are the transmission coefficient obtained numerically for the Kane-Mele model with a backscatterer at the edge. The red line is the fit to the effective model (cf. Eq. 8). (Right) Effective model parameters as a function of  $\lambda_{\text{imp}}$ .

malized BS amplitude for the edge electrons, and  $V_c$  the tunneling into and out of the bound states. The reflection coefficient for the effective model reads:

$$\mathcal{R}(\epsilon) = \left| \sum_{p=\pm 1} \frac{p}{\frac{iV_c^2}{(\epsilon + p\epsilon_0)\Delta} + (1 - p\frac{iV_B}{2\Delta})} \right|^2 \quad (11)$$

We have fitted the numerical results for the impurity system interacting with the edge of a 2DTI to this equation, as shown on the left panel of Fig. 4 for  $N = 2$ . The behavior of the fitted  $V_c$ ,  $V_B$ , and  $\epsilon_0$  as a function of  $\lambda_{\text{imp}}$ , is shown in the right panel. As expected from the above discussion,  $\epsilon_0$  decreases as  $\lambda_{\text{imp}} \rightarrow +\infty$ . Note also that  $V_c, V_B \ll \Delta$ . In passing, we note that for  $V_c = 0$ , the resonances disappear and the reflection coefficient becomes independent of the energy, which applies to an impurity located on the first atomic row ( $N = 1$ ).

Finally, we study the effect of electron interactions on the above picture. Interactions will be treated non-perturbatively using the bosonization method [20], and their characteristic energy scale  $e^2/a_0$  (where  $e$  is the electron charge) is assumed to be smaller than  $\Delta$ . Before considering interaction effects, we further project the effective 1D model in Eq. (8) must onto the subspace of excitations with energy  $\epsilon \approx \epsilon_F$  ( $\epsilon_F$  is Fermi energy). In particular, when  $\epsilon_F$  is away from the resonances at  $\pm\epsilon_0$ , the bound states can be integrated out. To leading order, this yields a renormalized backscattering amplitude:

$$V'_B \simeq V_B - \left[ \frac{V_c^2}{\epsilon_0 - \epsilon_F} + \frac{V_c^2}{\epsilon_0 + \epsilon_F} \right]. \quad (12)$$

Hence, the model reduces to the one studied by Kane and Fisher [12, 13] (see  $H_{KF}$  in Eq. 14 below), with the BS amplitude  $V_B$  replaced by  $V'_B$  from Eq. (12).

On the other hand, for  $\epsilon_F \simeq +\epsilon_0$  or  $\epsilon_F \simeq -\epsilon_0$ , the resonant level cannot be immediately integrated out, although the bound state further away can. Assuming (without loss of generality) that  $\epsilon_F \simeq -\epsilon_0$  yields the

following low-energy effective model:

$$H'_{\text{eff}} = H_{KF} + H_-[d, t_- \psi(0)] + \left( d^\dagger d - \frac{1}{2} \right) \times [U_F \psi^\dagger(0) \psi(0) + U_B \psi^\dagger(0) s^x \psi(0)], \quad (13)$$

$$H_{KF} = H_B + U \int dx \rho_R \rho_L. \quad (14)$$

Here we have also accounted for interactions between the edge electrons (with amplitude  $U$ ) and with the resonant level electron (with amplitudes  $U_F$  and  $U_B$ ). Furthermore, integrating out the non-resonant level at  $\epsilon = +\epsilon_0$  modifies the BS potential  $V_B - U_B/2$  in  $H'_{\text{eff}}$  by an amount  $\simeq V_c^2/(\epsilon_F - \epsilon_0) \simeq -V_c^2/2\epsilon_0$ . Forward scattering is also generated but it has been dropped since it can be eliminated by a unitary transformation [12, 20].

The Hamiltonian in  $H'_{\text{eff}}$  in Eq. (13) is very similar to a model of side-coupled level to an interacting 1D channel, which has been studied by Goldstein and Berkovits in Ref. [26]. Following these authors, after bosonizing [20] Eq. (13), we apply a unitary transformation and eliminate the forward interaction term  $\propto U_F$ , at the expense of renormalizing the scaling dimension ( $\Delta_c$ ) of the tunneling,  $O_c \propto V_c$ , where  $\langle O_c^\dagger(\tau) O_c(0) \rangle \sim \tau^{-2\Delta_T}$ , where  $\tau$  is the imaginary time and  $\Delta_T(K, U_F) = \frac{1}{4} \left[ K + K^{-1} \left( 1 - \frac{U_F K}{\pi v} \right)^2 \right]$ , where  $K = \sqrt{\frac{2\pi v_F - U}{2\pi v_F + U}}$  is the Luttinger parameter and  $v = v_F \sqrt{1 - \left( \frac{U}{2\pi v_F} \right)^2}$  the velocity of the edge plasmons [20]. Tunneling into the resonant state becomes relevant in the renormalization-group (RG) sense when  $\Delta_c(K, U_F) < 1$ . Thus, for weak to moderate repulsion (i.e.  $K \lesssim 1$ ), both tunneling  $V_c$  and the BS ( $\propto V_B, U_F$ ) renormalize to strong coupling and suppress the transmission across the impurity, as confirmed by the RG flows to 2nd order [26, 30]. Interestingly, for moderate attraction (i.e.  $K \gtrsim 1$ ), for which BS is *naively* irrelevant [12, 26], we have  $\Delta_c(K, U_F) < 1$ . Thus, tunneling flows to strong coupling and 2nd order RG flows [26, 30] show that the runaway flow of  $V_c$  drags along  $U_B$  and  $U_F$ , which leads to the narrowing of the anti-resonance in the transmission and suppression of conductance as  $T \rightarrow 0$ , also for weak to moderate attraction in the edge channel.

In summary, we have investigated the problem of an impurity inducing backscattering at the edge of a two-dimensional topological insulator (TI). By obtaining a solution of the scattering problem, we have derived the 1D effective low-energy Hamiltonian describing the system. Strong backscattering induces two discrete levels within the band gap, which couple to the (interacting) metallic edge(s). When the Fermi energy resonates with one of the levels, both moderately attractive or repulsive interactions suppress the transmission through the impurity. Off resonance, the system can be effectively described as an impurity in a Tomonaga-Luttinger liquid [12, 13, 18] with a renormalized backscattering potential. This picture should be robust in the presence of weak uniform Rashba spin-orbit, which will introduce an energy de-



pendence in the couplings of the effective model, Eq. (8), arising from the spin texture of the bulk and edge states. However, energy dependence is an irrelevant perturbation at low energies. Besides this, other model regimes and extensions to this work, such as multiple impurity problems, etc. will be explored elsewhere [34].

We thank L. Glazman, F. Guinea, Y.-H. Ho, C.-L. Huang, and X.-P. Zhang for useful discussions. M.A.C. gratefully acknowledges support by the Ministry of Science and Technology (Taiwan) under contract number NSC 102- 2112-M-007-024-MY5, and Taiwan's National Center of Theoretical Sciences (NCTS).

- 
- [1] M. Z. Hasan and C. L. Kane, Rev. Mod. Phys. **82**, 3045 (2010); X.-L. Qi and S.-C. Zhang, Rev. Mod. Phys. **83**, 1057 (2011).
  - [2] C. Wu, B. A. Bernevig, and S. C. Zhang, Phys. Rev. Lett. **96**, 106401 (2006).
  - [3] C. Xu and J. E. Moore, Phys. Rev. B **73**, 045322 (2006).
  - [4] G. Dolcetto, M. Sasseti, T.-L. Schmidt, Nuovo Cimento **39**, 113 (2016).
  - [5] A. Ström, H. Johannesson, and G. I. Japaridze, Phys. Rev. Lett. **104**, 256804 (2010); F. Crépin, J. C. Budich, F. Dolcini, P. Recher, and B. Trauzettel, Phys. Rev. B **86**, 121106 (2012); F. Geissler, F. Crépin, and B. Trauzettel, Phys. Rev. B **89**, 235136 (2014).
  - [6] M. König *et al.*, Science **318**, 766 (2007); A. Roth *et al.*, Science **325**, 294 (2009); K. C. Nowack *et al.*, Nat. Mater. **12**, 787 (2013); G. Grabecki *et al.*, Phys. Rev. B **88**, 165309 (2013); G. M. Gusev, *et al.*, Phys. Rev. B **89**, 125305 (2014); I. Knez, R.-R. Du, and G. Sullivan, Phys. Rev. Lett. **107**, 136603 (2011); K. Suzuki, Y. Harada, K. Onomitsu, and K. Muraki, Phys. Rev. B **87**, 235311 (2013); I. Knez *et al.*, Phys. Rev. Lett. **112**, 026602 (2014); E. M. Spanton *et al.*, Phys. Rev. Lett. **113**, 026804 (2014); A. F. Young, J. D. Sanchez-Yamagishi, B. Hunt, S. H. Choi, K. Watanabe, T. Taniguchi, R. C. Ashoori, and P. Jarillo-Herrero, Nature **505**, 528 (2014).
  - [7] T. L. Schmidt, S. Rachel, F. von Oppen, and L. I. Glazman, Phys. Rev. Lett. **108**, 156402 (2012); J. C. Budich, F. Dolcini, P. Recher, and B. Trauzettel, Phys. Rev. Lett. **108**, 086602 (2012); N. Lezmy, Y. Oreg, and M. Berkooz, Phys. Rev. B **85**, 235304 (2012); J. I. Väyrynen, M. Goldstein, and L. I. Glazman, Phys. Rev. Lett. **110**, 216402 (2013); J. I. Väyrynen, M. Goldstein, Y. Gefen, and L. I. Glazman, Phys. Rev. B **90**, 115309 (2014); N. Kainaris, I. V. Gornyi, S. T. Carr, and A. D. Mirlin Phys. Rev. B **90**, 075118 (2014).
  - [8] Y. Tanaka, A. Furusaki, and K. A. Matveev, Phys. Rev. Lett. **106**, 236402 (2011).
  - [9] L. Kimme, B. Rosenow, and A. Brataas, Phys. Rev. B **93**, 081301 (2016).
  - [10] E. Eriksson, A. Ström, G. Sharma, and H. Johannesson Phys. Rev. B **86**, 161103(R) (2012).
  - [11] J. Maciejko, C. Liu, Y. Oreg, X.-L. Qi, C. Wu, S.-C. Zhang, Phys. Rev. Lett. **102**, 256803 (2009).
  - [12] C. L. Kane and M. P. A. Fisher, Phys. Rev. Lett. **68**, 1220 (1992); Phys. Rev. B **46**, 15233 (1992).
  - [13] M. P. A. Fisher and L. Glazman in “Mesoscopic Electron Transport”, edited by L. Kowenhoven, G. Schön and L. Sohn, NATO ASI Series E, Kluwer Academic Publishers (Dordrecht, The Netherlands) (1997).
  - [14] L. I. Glazman, I. M. Ruzin, and B. I. Shklovskii, Phys. Rev. B **45**, 8454 (1992).
  - [15] S.-J. Qin, M. Fabrizio, and L. Yu Phys. Rev. B **54**, R9643(R) (1996).
  - [16] C. Rylands and N. Andrei, Phys. Rev. B **94**, 115142 (2016).
  - [17] Z. Yao, H. W. Ch. Postma, L. Balents, and C. Dekker, Nature (London) Nature **402**, 273-276 (1999).
  - [18] D. Yue, L. I. Glazman and K. A. Matveev, Phys. Rev. B **49**, 1966 (1994).
  - [19] J. S. Van Dyke and D. K. Morr Phys. Rev. B **93**, 081401(R) (2016); report arxiv:1609.01726 (2016).
  - [20] A. O. Gogolin, A. A. Nersesyan, A. M. Tsvelik, *Bosonization and Strongly Correlated Systems* Cambridge University Press (Cambridge, UK 1999). T. Giamarchi, *Quantum Physics in One-dimension*, Clarendon Press (Oxford, UK 2004).
  - [21] R. R. Biswas, and A. V. Balatsky, Phys. Rev. B **81**, 233405 (2010); W.-Y. Shan, J. Lu, H.-Z. Lu, and S.-Q. Shen, Phys. Rev. B **84**, 035307 (2011).
  - [22] J. R. Schieffer, Journal of Applied Physics **38**, 1143 (1967).
  - [23] A. Furusaki, Phys. Rev. B **57**, 7141 (1998).
  - [24] D. G. Polyakov, and I. V. Gornyi, Phys. Rev. B, **68**, 035421 (2003); Y. V. Nazarov and L. I. Glazman, Phys. Rev. Lett. **91**, 126804 (2003).
  - [25] I. V. Lerner, V. I. Yudson, and I. V. Yurkevich, Phys. Rev. Lett. **100**, 256805 (2008).
  - [26] M. Goldstein, and R. Berkovits, Phys. Rev. Lett. **104**, 106403 (2010).
  - [27] Z. Wang, Y. D. Chong J. D. Joannopoulos, and M. Soljai, Nature **461**, **772**, (2009).
  - [28] C. L. Kane and E. J. Mele, Phys. Rev. Lett. **95**, 226801 (2005); Phys. Rev. Lett. **95**, 146802 (2005).
  - [29] B. Zhou *et al.*, Phys. Rev. Lett. **101**, 246807 (2008).
  - [30] See supplementary material.
  - [31] G. Zhang *et al.*, Nanoscale, **6**, 3259 (2014).
  - [32] H. Doh, G. S. Jeon, and H. J. Choi, ArXiv:1408.4507 (2014).
  - [33] U. Fano, Phys. Rev. **124**, pp. 1866 (1961).
  - [34] J. H. Zheng and M. A. Cazalilla, *to be published*.

# Supplementary Material for “Strong Backscatterer at the Edge of a Two-dimensional Topological Insulator”

## INTRODUCTION

This supplementary contains details about our analytical approach to solve for the spectrum and the wavefunctions of both bulk and edge states for a generalized Kane-Mele (KM) model [1]. We shall consider two kinds of boundary conditions, corresponding to the zigzag and beard edges. The model Hamiltonian reads:

$$\hat{H}_0 = -t \sum_{\langle i,j \rangle} \hat{c}_i^\dagger \hat{c}_j - i\lambda_{\text{SO}} \sum_{\langle\langle i,j \rangle\rangle} \nu_{ij} \hat{c}_i^\dagger s^z \hat{c}_j + \lambda_v \sum_i \xi_i \hat{c}_i^\dagger \hat{c}_i. \quad (15)$$

We have included a staggered potential where  $\xi_i = +1$  for  $\mathbf{R}_i \in B$  and  $\xi_i = -1$  for  $\mathbf{R}_i \in A$  sublattice. This staggered potential can be used to drive a transition between a trivial and a topological phase. In the above expression,  $s^z$  denotes the spin and  $\sigma^z = (+, -)$  describes the sublattice pseudo spin components corresponding to the  $(B, A)$  sublattices. As discussed in the main text, there is a gauge degree of freedom for Fourier transformation of the fermion creation and destruction operators due to the bi-particle structure of lattice. The two types of edges considered below correspond to two different gauge choices: 1) Zigzag edge:  $\mathbf{r}_g = -(a/2\sqrt{3})\mathbf{e}_y$  and 2) Beard edge:  $\mathbf{r}_g = (a/\sqrt{3})\mathbf{e}_y$ .

## SPECTRUM OF EDGE STATES

First we shall derive the spectrum of the edge states for the zigzag edge. After Fourier transformation and taking into account that  $s^z$  is a good quantum number, we obtain the Schrödinger equation [2],

$$\mathcal{H}_0^s(\alpha, \hat{\beta})\Phi_s(k_x, y) = \epsilon\Phi_s(k_x, y), \quad (16)$$

where  $\alpha = k_x a/2$ , and  $\hat{\beta} = -i\frac{\sqrt{3}a}{2}\partial_y$ . Note that  $\mathcal{H}_0^s = \sum_i d_s^i \sigma^i$ , with  $d_s^x = -t(2\cos\alpha + \cos\hat{\beta})$ ,  $d_s^y = -t\sin\hat{\beta}$  and  $d_s^z = \lambda_v + s\lambda_{\text{SO}}(2\sin 2\alpha - 4\sin\alpha\cos\hat{\beta})$ , respectively. In the following, we will work in units where  $a = 1$ , for the sake of notational simplicity. In addition, we treat  $\hat{\beta}$  as an operator and  $\beta$  as its eigenvalues.

Looking for solutions of the form  $\Phi_s(k_x, y) = \chi_s e^{\kappa y}$ , where  $\beta = -i\frac{\sqrt{3}}{2}\kappa$  leads to the following secular equation:

$$\epsilon^2 - [\lambda_v + 2s\lambda_{\text{SO}}(\sin k_x - 2\sin \frac{k_x}{2} \cosh \frac{\sqrt{3}\kappa}{2})]^2 - t^2[1 + 4\cos \frac{k_x}{2} \cosh \frac{\sqrt{3}\kappa}{2}] - 4t^2(\cos \frac{k_x}{2})^2 = 0. \quad (17)$$

This equation relates  $\kappa$  and the eigenvalues,  $\epsilon$ . It is a quadratic equation of the variable  $f \equiv \cosh \frac{\sqrt{3}\kappa}{2}$ . By denoting  $X = -(4\lambda_{\text{SO}} \sin \frac{k_x}{2})^2$ ,  $Y = 8s\lambda_{\text{SO}} \sin \frac{k_x}{2} (\lambda_v + 2s\lambda_{\text{SO}} \sin k_x) - 4t^2 \cos \frac{k_x}{2}$ , and  $Z = \epsilon^2 - t^2 - 4t^2(\cos \frac{k_x}{2})^2 - (\lambda_v + 2s\lambda_{\text{SO}} \sin k_x)^2$ , we obtain the two roots:

$$f_{1,2} = (-Y \pm \sqrt{Y^2 - 4XZ})/2X \quad (18)$$

which implies there are four roots for  $\kappa$ , corresponding to  $\pm\kappa_{1,2}$  with  $\kappa_{1,2} = \frac{2}{\sqrt{3}} \cosh^{-1} f_{1,2}$ . The latter are all functions of the eigenvalue  $\epsilon$ . Note that for the edge states, we have that  $\text{Re } \kappa_{1,2} \neq 0$ . Thus, we use the convention that  $\text{Re } \kappa_{1,2} > 0$  for the function  $\kappa_{1,2} = \frac{2}{\sqrt{3}} \cosh^{-1} f_{1,2}$ .

Next we note that two linearly independent wavefunctions satisfy the open boundary conditions corresponding the zigzag edge, namely  $\Phi_s(k_x, \pm L/2) = 0$  for each value of  $\epsilon$  are  $g_c^1(k_x, y) - g_c^2(k_x, y)$  and  $g_s^1(k_x, y) - g_s^2(k_x, y)$ , where [2]

$$g_c^i(k_x, y) = \frac{\cosh(\kappa_i y)}{\cosh(\kappa_i L/2)}, \quad (19)$$

$$g_s^i(k_x, y) = \frac{\sinh(\kappa_i y)}{\sinh(\kappa_i L/2)} \quad (20)$$

Hence, the eigenfunctions can be expressed as the linear combination thereof. By introducing a  $2 \times 2$  matrix of coefficients  $\mathcal{L} = [l_{ij}]_{2 \times 2}$ , the eigenfunction can be written as follows:

$$\Phi_s(k_x, y) = \mathcal{L} \begin{bmatrix} g_c^1(k_x, y) - g_c^2(k_x, y) \\ g_s^1(k_x, y) - g_s^2(k_x, y) \end{bmatrix}. \quad (21)$$

Let us substitute this function back into the Schrödinger equation, Eq. (16). Because  $g_{c,s}^i$  are linearly independent, we obtain the following conditions relating the column vectors of the matrix  $\mathcal{L}$ :

$$\begin{aligned} \mathbf{L}_2 &= \tanh(\kappa_1 L/2) M_1 \mathbf{L}_1, & \mathbf{L}_2 &= \tanh(\kappa_2 L/2) M_2 \mathbf{L}_1, \\ \mathbf{L}_1 &= \frac{1}{\tanh(\kappa_1 L/2)} M_1 \mathbf{L}_2, & \mathbf{L}_1 &= \frac{1}{\tanh(\kappa_2 L/2)} M_2 \mathbf{L}_2, \end{aligned} \quad (22)$$

where  $\mathbf{L}_1 = (l_{11}, l_{21})^T$ ,  $\mathbf{L}_2 = (l_{12}, l_{22})^T$ ,  $M_i = \sigma^y \{ (-2t \cos \alpha - t \cos \beta_i) \sigma^x + (\lambda_v + 2s\lambda_{\text{SO}} \sin 2\alpha - 4s\lambda_{\text{SO}} \sin \alpha \cos \beta_i) \sigma^z - \epsilon \} / t \sin \beta_i$ , and  $\beta_i = -i \frac{\sqrt{3}}{2} \kappa_i$ , respectively. Note that, in the above derivation, we have used the fact  $\cos \hat{\beta} g_{c,s}^i(k_x, y) = \cos \beta_i g_{c,s}^i(k_x, y)$ ,  $\sin \hat{\beta} g_c^i(k_x, y) = \sin \beta_i \tanh(\kappa_i L/2) g_s^i(k_x, y)$  and  $\sin \hat{\beta} g_s^i(k_x, y) = \frac{\sin \beta_i}{\tanh(\kappa_i L/2)} g_c^i(k_x, y)$ .

The combinations of equations in the same column in Eq.(22) give the secular equation (17), which has been used to relate  $\kappa_i$  and spectrum  $\epsilon$ . The other two independent equations are obtained by combining diagonal terms in Eq.(22), which yields:

$$\mathbf{L}_2 = T M_1 M_2 \mathbf{L}_2 = \frac{1}{T} M_2 M_1 \mathbf{L}_2, \quad (23)$$

where  $T = \frac{\tanh(\kappa_1 L/2)}{\tanh(\kappa_2 L/2)}$ . Expressing  $\kappa_i$  as functions of  $\epsilon$ , this equation is exactly the constraint for spectrum  $\epsilon$ . In the following, we will solve this equation.

Eq.(23) implies  $M_t \mathbf{L}_2 = 0$ , where  $M_t \equiv T M_1 M_2 - \frac{1}{T} M_2 M_1$ . To have a nontrivial solution for  $\mathbf{L}_2$ , the condition  $\det M_t = 0$  is required. Explicitly,

$$M_t = \frac{-T [D_0 + D_x \sigma_x + D_y \sigma_y + D_z \sigma_z] + \frac{1}{T} [D_0 - D_x \sigma_x - D_y \sigma_y - D_z \sigma_z]}{t^2 \sin \beta_1 \sin \beta_2}, \quad (24)$$

where

$$D_x = t(\cos \beta_1 - \cos \beta_2) \epsilon \quad (25)$$

$$D_y = it(\lambda_v + 6s\lambda_{\text{SO}} \sin 2\alpha)(\cos \beta_1 - \cos \beta_2), \quad (26)$$

$$D_z = 4s\lambda_{\text{SO}} \sin \alpha (\cos \beta_1 - \cos \beta_2) \epsilon, \quad (27)$$

$$D_0 = t^2(2 \cos \alpha + \cos \beta_1)(2 \cos \alpha + \cos \beta_2) + (\lambda_v + 2s\lambda_{\text{SO}} \sin 2\alpha - 4s\lambda_{\text{SO}} \sin \alpha \cos \beta_1)(\lambda_v + 2s\lambda_{\text{SO}} \sin 2\alpha - 4s\lambda_{\text{SO}} \sin \alpha \cos \beta_2) - \epsilon^2. \quad (28)$$

Thus the condition  $\det M_t = 0$  becomes  $(T + \frac{1}{T})^2 = 4D_0^2/(D_0^2 - D_x^2 - D_y^2 - D_z^2)$ . Especially for  $L \rightarrow \infty$ , we have  $T = 1$  because  $\text{Re } \kappa_{1,2} > 0$ . Thus it further becomes  $D_x^2 + D_y^2 + D_z^2 = 0$ , which gives the spectra

$$\epsilon_s^\pm = \pm \frac{t(\lambda_v + 6s\lambda_{\text{SO}} \sin 2\alpha)}{\sqrt{t^2 + (4\lambda_{\text{SO}} \sin \alpha)^2}}. \quad (29)$$

Note that Eq.(23) gives an additional constraint for the spectra. From  $M_t \mathbf{L}_2 = 0$  and  $T = 1$ , we obtain  $(D_x \sigma_x + D_y \sigma_y + D_z \sigma_z) \mathbf{L}_2 = 0$ . Combining it with  $\mathbf{L}_2 = M_1 M_2 \mathbf{L}_2$  (Eq.(23)), we get the constraint

$$-D_0 = t^2 \sin \beta_1 \sin \beta_2. \quad (30)$$

The second constraint is  $\text{Re } \kappa_{1,2} > 0$ . These constraints restrict a region  $k_x \in [\Lambda_s^-, \Lambda_s^+]$ , where edge states exist. We show the resulted spectra in Fig.5.

## WAVEFUNCTIONS FOR A SEMI-INFINITE SYSTEM

To investigate the wavefunctions at one of edge, it is helpful to shift the position of system so that the system is on the upper half plane ( $0 \leq y \leq L$  with  $L \rightarrow \infty$ ).

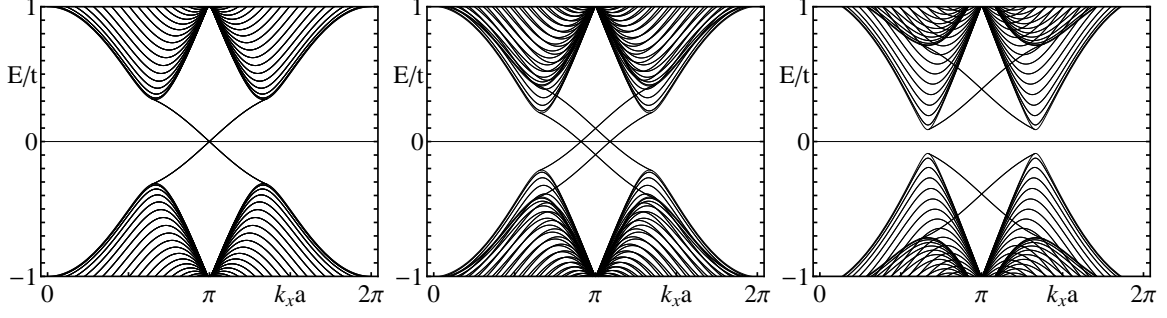


FIG. 5. Spectrum (Exact analytical solution). Left panel:  $\lambda_{\text{SO}} = 0.06t$  and  $\lambda_v = 0$ ; Central panel:  $\lambda_{\text{SO}} = 0.06t$  and  $\lambda_v = 0.1t < 3\sqrt{3}\lambda_{\text{SO}}$ ; Right panel:  $\lambda_{\text{SO}} = 0.06t$  and  $\lambda_v = 0.4t > 3\sqrt{3}\lambda_{\text{SO}}$ .

### Wavefunctions for edge states

For a semi-infinite system, the wavefunction satisfying the boundary condition  $\Phi_{sk_x}(0) = \Phi_{sk_x}(L \rightarrow \infty) = 0$  has a much simpler form

$$\Phi_{sk_x}(y) = C_s(k_x)\chi_s(k_x)(e^{-\kappa_{s,1}y} - e^{-\kappa_{s,2}y}). \quad (31)$$

The left problems are to solve the  $2 \times 1$  matrix  $\chi_s(k_x)$  and the normalization factor  $C_s(k_x)$ . For each  $k_x$ , we have obtain the spectra  $\epsilon_s$  and the ‘wave-vector’  $\kappa_{s,i} = \frac{2}{\sqrt{3}} \cosh^{-1} f_{s,i}$  with  $i = 1, 2$  in the last section. Substituting Eq. (31) into the Schrödinger Eq. (16), we obtain

$$\chi_s(k_x) = \begin{bmatrix} -[\mathcal{H}_0^s]_{12} / \{[\mathcal{H}_0^s]_{11} - \epsilon_s\} \\ 1 \end{bmatrix} \equiv \begin{bmatrix} \chi_{s,1} \\ 1 \end{bmatrix}. \quad (32)$$

Explicitly,

$$\chi_{s,1} = \frac{2t \cos \frac{k_x}{2} + t \exp(\sqrt{3}\kappa_{s,1}/2)}{\lambda_v + 2s\lambda_{\text{SO}}[\sin k_x - 2 \sin(k_x/2) \cosh(\sqrt{3}\kappa_{s,1}/2)] - \epsilon_s} \quad (33)$$

Note that the system is a lattice structure, and therefore the wavefunction is defined on the discrete lattice points only:

$$\psi_{sk_x}(n) = C_s(k_x)\chi_s(k_x)(e^{-\kappa_{s,1}ny_0} - e^{-\kappa_{s,2}ny_0}), \quad (34)$$

where  $y_0 = \sqrt{3}a/2$ . The normalization factor is

$$C_s(k_x) = (|\chi_{s,1}|^2 + 1)^{-1/2} C_s^0(k_x) \quad (35)$$

where

$$C_s^0(k_x) = [\Upsilon(2 \text{Re } \kappa_{s,1}) + \Upsilon(2 \text{Re } \kappa_{s,2}) - \Upsilon(\kappa_{s,1}^* + \kappa_{s,2}) - \Upsilon(\kappa_{s,1} + \kappa_{s,2}^*)]^{-1/2} \quad (36)$$

where the function  $\Upsilon(k) \equiv 1/[1 - \exp(-ky_0)]$ . Upon denoting  $\Phi_{sk_x,\sigma}(\mathbf{r})$  as the  $\sigma$  components of  $\Phi_{sk_x}(\mathbf{r})$ , we find  $|\Phi_{sk_x,+}(\mathbf{r})|^2 \gg |\Phi_{sk_x,-}(\mathbf{r})|^2$  for the case  $\lambda_v = 0$  and  $\lambda_{\text{SO}} \ll t$ , which suggesting the bottom edge states ‘prefer’ B-sublattice.

### Wavefunctions for Bulk States

For the bulk states with periodic boundary conditions, crystal momentum  $\mathbf{k} = (k_x, k_y)$  is treated as good quantum number in both the  $x$ -direction and  $y$ -direction. Thus, upon setting  $\kappa = ik_y$  in Eq. (17) (with  $\beta = \frac{\sqrt{3}k_y}{2}$ ), we obtain the (bulk) dispersion:

$$E_{s\eta}(\mathbf{k}) = E_{s\eta}(k_x, k_y) = \eta \sqrt{t^2 + 4t^2 \cos \alpha \cos \beta + 4t^2 \cos^2 \alpha + [\lambda_v + 2s\lambda_{\text{SO}}(\sin 2\alpha - 2 \sin \alpha \cos \beta)]^2}, \quad (37)$$



where  $s, \eta = \pm 1$ .

However, for open boundary conditions and in the limit  $L \rightarrow \infty$ , the spectrum of bulk state is not modified from the above form because the boundary effects become negligible in the thermodynamic limit. On other hand, wavefunctions are modified and become different from Bloch waves because of the scattering with the boundary. Thus, from the secular equation (17), for each  $\kappa_1 = ik_y$  ( $k_y$  is real) and thus  $f_1 \equiv \cos \frac{\sqrt{3}k_y}{2}$ , we can find another root,  $f_2 = -\frac{Y}{X} - f_1$ . In total four different roots for  $\kappa$  exist, i.e.,  $\pm\kappa_{1,2}$  with  $\kappa_{1,2} = \frac{2}{\sqrt{3}} \cosh^{-1} f_{1,2}$ , corresponding to a same energy  $\epsilon$ . Note that  $f_1$  and thus  $f_2$  are real. Thus there are two different cases: 1)  $|f_2| > 1$ , the plane wave decays at the edge; and 2)  $|f_2| \leq 1$ , different modes interference with each other:

- **Case 1:** For  $|f_2| > 1$ , we have  $\kappa_2 = \frac{2}{\sqrt{3}} \cosh^{-1} f_2$  with  $\text{Re } \kappa_2 > 0$ . Thus the full solutions of the secular equation (17) for  $\kappa$  are  $\pm ik_y$  and  $\pm\kappa_2$ . The mode  $\sim e^{\kappa_2 y}$  diverges for  $y \rightarrow \infty$ , so it will not emerge and there are only there modes left:  $e^{\pm\kappa_1 y}$  and  $e^{-\kappa_2 y}$ . After using the boundary condition  $\Phi_{s\eta, \mathbf{k}}(y=0) = 0$ , only two linear independent wavefunctions are left. The general wavefunction has the following form:

$$\Phi_{s\eta, \mathbf{k}}(y) = \frac{1}{\sqrt{N_y}} C_{s\eta}(\mathbf{k}) \mathcal{L} \begin{bmatrix} \exp(ik_y y) - \exp(-\kappa_2 y) \\ \exp(-ik_y y) - \exp(-\kappa_2 y) \end{bmatrix}, \quad (38)$$

where  $\mathcal{L} = [l_{ij}]_{2 \times 2}$  is a  $2 \times 2$  matrix, and  $C_{s\eta}(\mathbf{k})$  is the normalization constant. Obviously, such a kind of wavefunction is a combination of extended state and local state, which decays at the edge.

Now we need to calculate out the matrix  $\mathcal{L}$ . Substituting Eq.(38) into Schrödinger equation (16), and using

the fact that  $\exp(\pm ik_y y)$  and  $\exp(-\kappa_2 y)$  are linear independent, we obtain the following results:  $\mathbf{L}_1 = c_1 \begin{bmatrix} l_1 \\ 1 \end{bmatrix}$ ,

$\mathbf{L}_2 = c_2 \begin{bmatrix} l_1^* \\ 1 \end{bmatrix}$ , and  $\mathbf{L}_1 + \mathbf{L}_2 = \begin{bmatrix} l_2 \\ 1 \end{bmatrix}$ , where  $\beta_1 = \frac{\sqrt{3}}{2} k_y$ ,  $\beta_2 = i \frac{\sqrt{3}}{2} \kappa_2$ ,  $\mathbf{L}_1 = (l_{11}, l_{21})^T$ ,  $\mathbf{L}_2 = (l_{12}, l_{22})^T$ ,  $c_1, c_2$  are constants, and  $l_i = -[\mathcal{H}_0^s(\alpha, \beta_i)]_{12} / \{[\mathcal{H}_0^s(\alpha, \beta_i)]_{11} - E_{s\eta}(\mathbf{k})\}$ . Solving these equations, we find  $c_1 = \frac{l_2 - l_1^*}{l_1 - l_1^*}$  and  $c_2 = \frac{-l_2 + l_1}{l_1 - l_1^*}$ .

The next step is to calculate the normalization coefficient  $C_{s\eta}(\mathbf{k})$ . For large  $L$  limit,  $\exp(-\kappa_2 y)$  does not influence normalization. Using the orthogonality of  $\exp(\pm ik_y y)$ , we obtain

$$C_{s\eta}(\mathbf{k}) = \frac{1}{\sqrt{|c_1|^2 + |c_2|^2} \sqrt{|l_1|^2 + 1}}. \quad (39)$$

As a result, in real space, we have

$$\Phi_{s\eta, \mathbf{k}}(n) = \frac{1}{\sqrt{N_y}} C_{s\eta}(\mathbf{k}) \mathcal{L} \begin{bmatrix} \exp(ik_y n y_0) - \exp(-\kappa_2 n y_0) \\ \exp(-ik_y n y_0) - \exp(-\kappa_2 n y_0) \end{bmatrix}, \quad (40)$$

- **Case 2:** For  $|f_2| \leq 1$ , we have  $\kappa_2 = \frac{2}{\sqrt{3}} \cosh^{-1} f_2 = ik'_y$  with  $k'_y \geq 0$ . The full solutions of the secular equation (17) for  $\kappa$  are  $\pm ik_y$  and  $\pm ik'_y$ . The boundary conditions  $\Phi_{s\eta, \mathbf{k}}(y=0) = 0$  require these four running waves inference with each other, and thus there are only three linear independent wavefunctions. Following the method used in previous case, we can construct the eigenfunctions by combining the three wavefunctions. However, we shall proceed in a different way here. Similar to the previous case, there is one eigenfunction,

$$|1\rangle = \frac{1}{\sqrt{N_y}} C_{s\eta}(\mathbf{k}) \mathcal{L} \begin{bmatrix} \exp(ik_y y) - \exp(-ik'_y y) \\ \exp(-ik_y y) - \exp(-ik'_y y) \end{bmatrix}, \quad (41)$$

where  $\mathcal{L}$  is same as the one in Eq. (38) except for the replacement of  $\kappa_2$  with  $ik'_y$  and thus the normalization becomes:

$$C_{s\eta}(\mathbf{k}) = \frac{1}{\sqrt{(|c_1|^2 + |c_2|^2)(|l_1|^2 + 1) + (|l_2|^2 + 1)}}. \quad (42)$$

The second eigenstate  $|2\rangle$  can be obtained by the replacements:  $k_y \longleftrightarrow k'_y$  (which imply that  $l_2 \longleftrightarrow l_1^*$ ). We denote the corresponding parameters as  $\mathbf{L}'_1, \mathbf{L}'_2, c'_1, c'_2$  and  $C_{s\eta}(\mathbf{k}')$ . Note that these two eigenstates are not orthogonal.

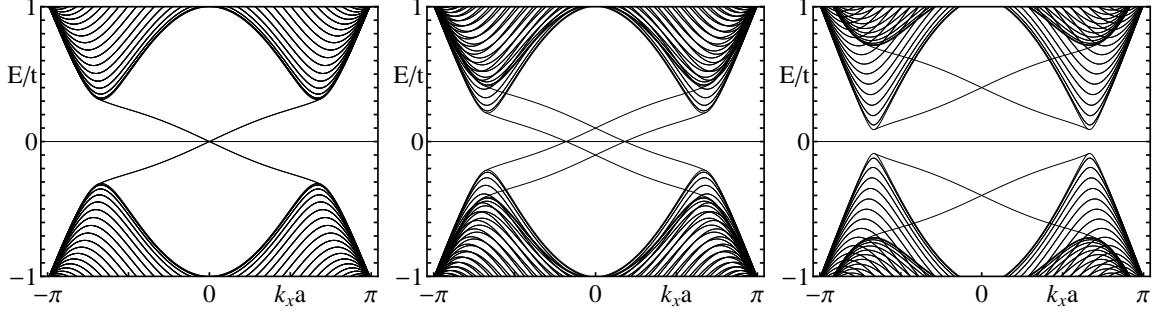


FIG. 6. Spectrum (Exact analytical solution). Left panel:  $\lambda_{SO} = 0.06t$  and  $\lambda_v = 0$ ; Central panel:  $\lambda_{SO} = 0.06t$  and  $\lambda_v = 0.1t < 3\sqrt{3}\lambda_{SO}$ ; Right panel:  $\lambda_{SO} = 0.06t$  and  $\lambda_v = 0.4t > 3\sqrt{3}\lambda_{SO}$ .

In the following, we construct an orthogonal and symmetric basis by means of

$$|+\rangle = |1\rangle + \vartheta |2\rangle, \quad |-\rangle = |2\rangle + \vartheta |1\rangle. \quad (43)$$

Using the orthogonality condition together with  $\langle 1 | 1 \rangle = \langle 2 | 2 \rangle = 1$ , we obtain

$$|\vartheta|^2 = 1, \quad \text{Re } \vartheta = -\text{Re } \langle 1 | 2 \rangle, \quad (44)$$

where  $\langle 1 | 2 \rangle = C_{s\eta}(\mathbf{k})C_{s\eta}(\mathbf{k}')[-c_2^*(|l_1|^2+1)-c_2'(|l_2|^2+1)]$ . We use the convention that  $\text{Im } \vartheta = \sqrt{1 - (\text{Re } \vartheta)^2} \geq 0$ , and finally, we obtain the orthonormalized wavefunctions

$$\Phi_{s\eta\mathbf{k}}(n) = \frac{1}{\sqrt{2 + 2\text{Re}[\vartheta \langle 1 | 2 \rangle]}} |+\rangle, \quad \Phi_{s\eta\mathbf{k}'}(n) = \frac{1}{\sqrt{2 + 2\text{Re}[\vartheta \langle 2 | 1 \rangle]}} |-\rangle. \quad (45)$$

### Green's function for the Kane-Mele model in a semi-infinite system

So far, we have obtained the eigenvalues and the complete set of eigenfunctions for the model of Eq. 15. Hence, the Green's function can be expressed in terms of them:

$$\hat{G}_0(\epsilon) = \sum_{\mathbf{k}, s, \eta} \frac{|\mathbf{k}, s, \eta\rangle \langle \mathbf{k}, s, \eta|}{\epsilon + i0^+ - E_{s\eta}(\mathbf{k})} + \sum_{k_x, s} \frac{|k_x, s\rangle \langle k_x, s|}{\epsilon + i0^+ - \epsilon_s(k_x)}, \quad (46)$$

where  $|\mathbf{k}, s, \eta\rangle = \Phi_{s\eta\mathbf{k}}$ . In the real space,  $G_{0,\sigma\sigma'}^s(\mathbf{r}, \mathbf{r}', \epsilon) = \langle \mathbf{r}, s, \sigma | \hat{G}_0(\epsilon) | \mathbf{r}', s, \sigma' \rangle$ , where  $\sigma = \pm 1$  represents the different components of  $\sigma^z$ . Thus, using  $\langle \mathbf{r}, s, \sigma | \mathbf{k}, s, \eta \rangle = \Phi_{s\eta\mathbf{k},\sigma}(\mathbf{r})$  and  $\langle \mathbf{r}, s, \sigma | k_x, s \rangle = \Phi_{sk_x,\sigma}(\mathbf{r})$ , where  $\Phi_{s\eta\mathbf{k},\sigma}(\mathbf{r})$  and  $\Phi_{sk_x,\sigma}(\mathbf{r})$  are the  $\sigma$  components of  $\Phi_{s\eta\mathbf{k}}(\mathbf{r})$  and  $\Phi_{sk_x}(\mathbf{r})$  respectively, we have

$$G_{0,\sigma\sigma'}^s(\mathbf{r}, \mathbf{r}', \epsilon) = \sum_{\mathbf{k}, \eta} \frac{\Phi_{s\eta\mathbf{k},\sigma}(\mathbf{r}) \Phi_{s\eta\mathbf{k},\sigma'}^*(\mathbf{r}')}{\epsilon + i0^+ - E_{s\eta}(\mathbf{k})} + \sum_{k_x} \frac{\Phi_{sk_x,\sigma}(\mathbf{r}) \Phi_{sk_x,\sigma'}^*(\mathbf{r}')}{\epsilon + i0^+ - \epsilon_s(k_x)}. \quad (47)$$

### SPECTRUM FOR BEARD EDGE

For beard edge, using the gauge  $\mathbf{r}_g = (a/\sqrt{3})\mathbf{e}_y$ , and following the same steps as for the zigzag case, we obtain the spectrum for edge state,

$$\epsilon_s^\pm = \pm \frac{t[2s\lambda_{SO} \sin \alpha + \cos \alpha (\lambda_v + 2s\lambda_{SO} \sin 2\alpha)]}{\sqrt{(t \cos \alpha)^2 + (2\lambda_{SO} \sin \alpha)^2}}. \quad (48)$$

In this case, the constraint becomes  $-D_0 = 4t^2 \cos^2 \alpha \sin \beta_1 \sin \beta_2$ , where  $D_0 = t^2 w_1 w_2 + u_1 u_2 - \epsilon^2$ ,  $w_i = 1 + 2 \cos \alpha \cos \beta_i$  and  $u_i = \lambda_v + 2s\lambda_{SO} \sin 2\alpha - 4s\lambda_{SO} \sin \alpha \cos \beta_i$ . The resulting band structure is shown in Fig. 6. Note that the edge states intersect at  $k_x = 0$  [3].

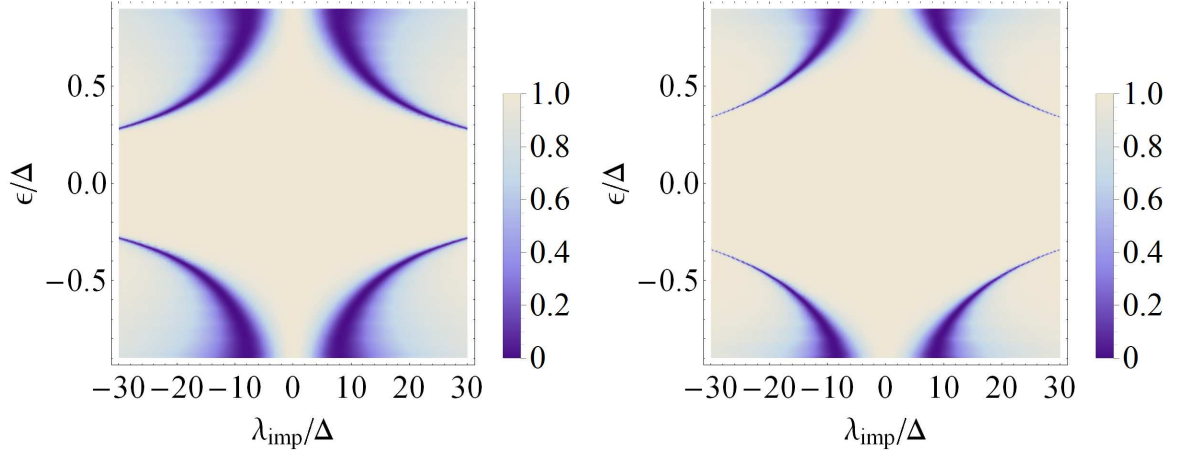


FIG. 7. Transmission coefficient  $\mathcal{T}(\epsilon)$  for an impurity on a B sublattice site on the first atomic row (i.e.  $N = 3$ ) (left),  $N = 4$  (right) (The spin-orbit coupling is  $\lambda_{SO} = 0.06 t$ ).

### TRANSMISSION COEFFICIENTS FOR INNER ROWS

The transmission coefficient  $\mathcal{T}(\epsilon)$  as a function of the impurity strength  $\lambda_{\text{imp}}$  and the electron energy, for an impurity on the B sublattice site on the rows  $N = 3$  and  $N = 4$  is shown in Fig. 7.

### RENORMALIZATION GROUP ANALYSIS

Next, in order to deal with the effects of interactions in a nonperturbative way, we shall rely upon the bosonization technique. The resulting model is analyzed using the renormalization-group (RG) following Ref. 4.

Using bosonization, the electron field operator for the right ( $R$ ) and left moving ( $L$ ) edge electron can be expressed in terms of a set of bosonic fields  $\theta(x)$  and  $\phi(x)$  as follows:

$$\psi_{R(L)}(x) = \frac{U_{R(L)}}{\sqrt{2\pi v \xi}} e^{-i[\pm\phi(x) - \theta(x)]}, \quad (49)$$

where  $\xi$  is a short-distance cutoff,  $v = v_F(1 - \frac{U}{2\pi v_F})^{1/2}$  is the plasmon velocity,  $U_R$  and  $U_L$  are the so-called Klein factors satisfying  $\{U_r, U_{r'}\} = 2\delta_{r,r'}$ , which allows to satisfy the anti-commutation relations between the two fermion chiralities  $R$  and  $L$ . The bosonic fields obey  $[\phi(x), \theta(x')] = i\frac{\pi}{2}\text{sgn}(x' - x)$ . The chiral densities are given by

$$\rho_{R(L)}(x) = -\frac{1}{2\pi} (\partial_x \phi \mp \partial_x \theta). \quad (50)$$

After bosonizing the low energy effective model and upon applying a unitary transformation generated by  $S = \exp[i\zeta\theta_0]$  with  $\zeta = \delta_F(d^\dagger d - \frac{1}{2})$ ,  $\delta_F = \frac{KU_F}{\pi v}$ , and using the factor  $e^{-i\zeta\theta(0)}\partial_x\phi(x)e^{i\zeta\theta(0)} = \partial_x\phi(x) - i\zeta[\theta(0), \partial_x\phi(x)] = \partial_x\phi(x) + \zeta\pi\delta(x)$ , the forward scattering term  $\propto U_F$  can be eliminated from  $H_{\text{eff}}$  (cf. Eq. 13 in the main text), and the resulting Hamiltonian,  $H''_{\text{eff}} = S^\dagger H'_{\text{eff}} S$  reads[4]:

$$H''_{\text{eff}} = H_* + \frac{v_B}{\xi} [U_R U_L e^{2i\phi_0} + h.c.] + 2\frac{y_B}{\xi} (d^\dagger d - \frac{1}{2}) [U_R U_L e^{2i\phi_0} + h.c.] \\ + \frac{y_t}{\xi} [d^\dagger (U_R e^{-i(\phi_0 - \lambda\theta_0)} - U_L e^{-i(-\phi_0 - \lambda\theta_0)}) + h.c.], \quad (51)$$

$$H_* = \frac{v}{2\pi} \int dx [K (\partial_x \theta)^2 + K^{-1} (\partial_x \phi)^2] - \varepsilon_0 (d^\dagger d - \frac{1}{2}). \quad (52)$$

where  $\lambda = 1 - \delta_F$ ,  $\phi_0 = \phi(0)$ ,  $\theta_0 = \theta(0)$ ,  $v_B$ ,  $y_B$ ,  $y_t$  are dimensionless couplings, and  $K$  is the so-called Luttinger parameter and  $v$  is the edge plasmon velocity. Here we also use the factor  $e^{-i\zeta\theta_0} d^\dagger e^{i\zeta\theta_0} = d^\dagger \exp[-i\delta_F\theta_0]$ . In the above equation  $\varepsilon_0$  denotes the distance of the (low-energy) bound state from the Fermi energy  $\epsilon_F$ . In what follows we focus on the resonant case for which  $\epsilon_0 = 0$ .

Taking into account the scaling behavior

$$\left\langle e^{2i\phi_0(\tau')} e^{-2i\phi_0(\tau)} \right\rangle \sim |\tau' - \tau|^{-2K} \quad (53)$$

and

$$\left\langle e^{i[\phi_0(\tau') - \lambda\theta_0(\tau')] } e^{-i[\phi_0(\tau) - \lambda\theta_0(\tau)]} \right\rangle \sim |\tau' - \tau|^{-K/2 - \lambda^2 K^{-1}/2}, \quad (54)$$

and their operator product expansions (OPE), using Cardy's approach [5], we arrive at the following set of RG equations valid to second order in the couplings describing backscattering ( $y_B$ ) and tunneling in and out of the resonant level:

$$\frac{dy_B}{d\ln\xi} = (1 - K) y_B + y_t^2. \quad (55)$$

$$\frac{dy_t}{d\ln\xi} = [1 - K/4 - (1 - \delta_F)^2 K^{-1}/4] y_t + y_t(y_B + v_B), \quad (56)$$

$$\frac{d\delta_F}{d\ln\xi} = 4(1 - \delta_F) y_t^2, \quad (57)$$

$$\frac{dv_B}{d\ln\xi} = (1 - K) v_B. \quad (58)$$

These RG equations are similar to the ones derived in Ref. 4. They show that for weak to moderate attractive interactions (i.e.  $K > 1$ ), the tunneling operator  $\propto y_t$  is flows to strong coupling. On the other hand, both the backscattering interaction ( $\propto y_B$ ) and potential ( $\propto v_B$ ) will be initially suppressed. Eventually, the runaway of  $y_t$  drags along  $\delta_F$  and  $y_B$ , quickly driving the forward interaction with the level to its fixed point  $\delta_F^* = 1$ . As a result, the transmission through the impurity will be suppressed [4], as discussed in the main text.

---

[1] C. L. Kane and E. J. Mele, Phys. Rev. Lett. **95**, 146802 (2005).

[2] B. Zhou, *et al.*, Phys. Rev. Lett. **101**, 246807 (2008).

[3] G. Zhang *et al.*, Nanoscale, **6**, 3259 (2014).

[4] M. Goldstein, and R. Berkovits, Phys. Rev. Lett. **104**, 106403 (2010).

[5] J. Cardy, *Scaling and Renormalization in Statistical Physics*, Cambridge University Press (Cambridge, UK, 1996).